J. Fluid Mech. (1987), *vol.* 183, *pp.* 25–44
Printed in Great Britain

Boundary mixing in a rotating, stratified fluid

By G. N. IVEY

Research School of Earth Sciences, Australian National University, GPO Box 4, Canberra, ACT 2601, Australia

(Received 16 April 1986 and in revised form 29 October 1986)

An earlier laboratory experiment of Ivey & Corcos (1982) on boundary mixing in a stratified fluid was extended by including the effects of rotation. An axisymmetric version of the original laboratory experiments was constructed and a series of experiments conducted on a rotating table with the tank filled with salt-stratified solution. The combination of vertical mixing at the boundary and horizontal mixing by mesoscale eddies lead to the weakening of the interior density gradient. While the mechanisms were thus complex, the experiments demonstrated that the boundary-mixing process may be parameterized by a relatively simple formulation dependent upon the turbulence properties at the boundary and the tank dimensions.

1. Introduction

The suggestion that mixing in the deep ocean could be due predominantly to boundary mixing was first made in a seminal paper by Munk (1966). Field observations have been made subsequently both in lakes (Caldwell, Brubaker & Neal 1978; Marmorino, Danos & Maki 1980; Imberger 1985) and in the oceans (Wunsch 1972; Armi 1978; Gregg & Sanford 1980; Dickson & McCave 1986) of the signatures of boundary-mixing processes. In lakes the boundary mixing is likely to be driven by either internal seiching or inflows. In the oceans, the boundary mixing is likely to be driven by either the mean flow interacting with the bottom (Armi 1978, 1979) or by bottom reflection of internal waves (Eriksen 1985). The latter mechanism appears more likely on the basis of energy arguments (Garrett 1979; Eriksen 1985), although further work is required to resolve these issues. In terms of the overall basin-scale mixing, McDougall's (1986) recent use of field data to study mixing along neutral surfaces in the North Atlantic led him to suggest that, if his results could be generalized to the World Ocean, then boundary mixing must indeed be important throughout the deep ocean.

What remained unclear from these studies is the mechanism by which the effects of boundary mixing are communicated to the interior. Whether the driving mechanism is a mean flow or internal wave bottom reflection the initial effect is the same: a near boundary-mixing event creates a local increase in potential energy relative to the interior. The subsequent along-isopycnal adjustment must ultimately lead to vertical fluxes in the interior.

In order to study this lateral along-isopycnal adjustment in response to forcing at the boundaries, Ivey & Corcos (1982) (hereinafter referred to as IC) conducted an initial laboratory experiment. Boundary mixing was simulated by vertically oscillating a grid placed flush with one vertical endwall of a rectangular tank filled with a salt-stratified solution. The oscillation of the grid created turbulence and the effect of the stratification was to confine the turbulence to a region adjacent to the grid

of finite width l_F. The interior of the laboratory tank remained quiescent. Nevertheless, the initial density gradient was steadily weakened uniformly throughout the tank. This adjustment was accomplished by a tank- or basin-scale circulation driven by fluid pumped out of the turbulent region and the bounded nature of the container resulted in the weakening of the interior density gradient by slow vertical advection.

In the oceans, the horizontal scales are sufficiently large that rotation must affect this lateral adjustment. With this application in mind, a laboratory experiment has been designed where both the scale of the turbulent region at the boundary and the internal Rossby deformation radius characterizing the interior are small compared to the tank dimensions. The purpose of this study is then to examine the effect of rotation on the boundary-mixing mechanism.

2. Laboratory experiments

An axisymmetric version of the original experiments by IC was constructed and the entire experiment placed on a direct-drive rotating table. The experiments were performed in a 1 m diameter Perspex tank. A vertically-oscillating cylindrical grid, with an external diameter of 11 cm, was mounted vertically in the centre of the tank and oscillated via an eccentric crank and arm mechanism. Roughness elements were created by machining a regular series of horizontal grooves around the circumference of the cylinder (each groove had a 1.27 cm square cross-section and there was a 2.54 cm centreline to centreline spacing along the axis of the cylinder). The grid therefore resembled a cylindrical version of the planar grid used by IC. The annular gap between the central cylindrical grid and the outer tank wall was filled to a depth of either 30 or 40 cm with a salt-stratified solution through fluid slip rings while the rotating table was spinning. In all but the first few experiments, a rigid lid was added to eliminate surface wave activity.

Flow visualization was accomplished with dye injection directly through the grid. Dyed fluid was fed through fluid slip rings onto the table, passed through a manifold system inside the hollow grid, and eventually out through one of five annular sponge rubber rings inset into consecutive grooves in the grid itself. The depth of dye release was chosen to coincide with the interface of the two-layer stratification with which all experiments were commenced. A record of the experiments was made with both 35 mm and video cameras mounted on a circular plate 2 m above the table and bolted to a frame attached to the rotating table.

The evolution of the salinity, and hence density gradient, was monitored with two four-wire micro-conductivity probes. The two probes, mounted at approximately one-third and two-thirds of the tank radius, were oriented vertically and could be traversed simultaneously up and down with a small stepping motor. The probes were sampled at 20 Hz, output voltages were logged directly onto a small laboratory computer, and the effective spatial resolution was about 0.5 mm in the vertical while the resolution in density was about 0.01 σ units. The output probe voltages were calibrated against an Anton Paar digital densimeter. The entire system thus yielded fine resolution of the evolution of the mean density profiles in the tank as the mixing progressed.

3. Experimental results

3.1. *General description*

An experiment was performed by first filling the tank with a layer of fresh water and setting the table in motion at the desired speed of rotation (in the anticlockwise direction in all runs). Once the first layer was in solid-body rotation, a second layer of salt water was slowly pumped onto the table through the fluid slip rings. This fluid was slowly added beneath the fresh-water layer through two pipes placed against the outer walls with their outlets near the bottom of the 1 m diameter tank. A list of parameter values for each run is given in table 1. Once filling was completed, the tank contained a two-layer stratification in solid body rotation and the experiment commenced with the initiation of the grid stirring.

The oscillation of the grid created a localized mixed region at the interface between the initial two layers. The resulting buoyancy forces caused a symmetrical, radial collapse of this mixed region. In order to conserve angular momentum in the rotating reference frame, the mixed region acquired an azimuthal velocity as it collapsed radially and it formed an anticyclonic vortex around the grid. This axisymmetric flow became, in turn, unstable to non-axisymmetric disturbances which manifested themselves as growing perturbations to the initially circular shape of the vortex.

Figure 1 provides a sequence of photographs from one experiment illustrating this process. The dye injected through the grid was observed to be essentially confined to the radially spreading mixed region which grew away from the grid and out along the original density interface (see the schematic in figure 5, for example). Thirteen rotation periods after the commencement of stirring (figure 1*a*), the growing non-axisymmetric disturbances are clearly visible on the periphery of the mixed region. After 26 rotation periods (figure 1*b*), the instability has grown and indicates an azimuthal wavenumber of 3 as the entire pattern drifts anticyclonically (figure 1*c*). The combination of the continual production of mixed fluid by grid stirring and the interaction of the rotational instabilities leads to a break-up of this structure (figure 1*c*) and the subsequent rapid radial spread of the mixed fluid across the entire container after some 179 rotation periods (figure 1*d*).

A photographic sequence from an experiment done at a higher rotation rate graphically illustrates the role of rotation in this radial mixing (see figure 2). After 79 rotation periods (figure 2*a*), the initial regular disturbances have broken down and their subsequent interaction has produced a field of chaotic eddy motions, although the dye cloud has only spread partially across the tank. These eddies persist and, even after 286 rotation periods (figure 2*d*), the dyed, mixed fluid still has not spread completely over the tank width. It is clear that rotation is important in the growth of the non-axisymmetric instability on the initial anticyclone of mixed fluid around the grid and, as described in detail in §3.2 below, in the subsequent spreading of the mixed region.

The net effect of the combination of vertical mixing due to grid stirring and the subsequent radial distribution of this mixed fluid across the tank by the mesoscale eddying motions lead to a weakening of the interior density gradient (figure 3). The dye introduced through the grid was observed to be mixed across the tank width, thus creating a dyed interfacial layer which subsequently thickened at the expense of the upper and lower homogeneous (undyed) layers. This behaviour was in close accord with the thickening of the original sharp density interface shown in figure 3 as the interior density gradient was steadily weakened – in this case, in an apparently uniform manner throughout the tank. The density profiles have the appearance of

Run	Table rotation rate $\Omega(\mathrm{rs}^{-1})$	Grid frequency $\omega(\mathrm{rs}^{-1})$	Grid amplitude a(cm)	Initial stratification		
				h_1(cm)	h_2(cm)	$\Delta\rho(\mathrm{kg\ m}^{-3})$
1	1.5	37.1	0.50	20.0	20.0	26.1
2	0.5	39.0	0.50	19.0	19.0	25.0
3	3.0	26.1	1.05	12.5	16.2	11.1
4	3.0	38.2	1.05	12.0	16.0	12.1
5	1.0	36.6	1.05	20.0	20.0	5.3
6	1.0	40.8	0.75	20.0	20.0	24.7
7	1.0	40.0	0.75	20.0	20.0	6.2
8	0.5	38.1	0.51	20.0	20.0	6.3
9	1.5	37.7	0.51	20.0	20.0	26.1
10	1.0	39.6	0.75	20.0	20.0	10.6
11	2.0	39.6	0.50	15.0	15.0	6.7
12	3.0	39.6	0.52	15.0	15.0	7.5
13	2.5	39.2	0.52	15.0	15.0	6.0
14	0.0	38.9	0.52	15.0	15.0	6.0

TABLE 1. Summary of the experimental programme

an apparent one-dimensional vertical turbulent mixing process, although the observations indicated it was in fact a very two-dimensional process (with azimuthal symmetry) with rotation affecting the horizontal adjustment. At higher rotation rates, the weakening of the vertical density gradient was no longer uniform in the radial direction (figure 4), and radial density gradients developed. In order to quantify these differing mean behaviours it is necessary to examine firstly the radial or horizontal adjustment process.

3.2. *Horizontal mixing*

As the conductivity data revealed, the radially collapsing mixed region marked by the dye was not well-mixed. Rather, it was only partly mixed and as shown schematically in figure 5, this suggests the following definition for a representative density anomaly $\overline{\Delta\rho}$ between this radially propagating fluid and the environment

$$\overline{\Delta\rho} = \frac{1}{h}\int_{-\frac{1}{2}h}^{\frac{1}{2}h} |\rho_a - \rho_b|\,\mathrm{d}z,$$

where ρ_a and ρ_b are the densities at corresponding heights as measured along profiles a and b respectively. The ratio $(2\overline{\Delta\rho}/(\rho_2-\rho_1))$, where ρ_1 and ρ_2 were the densities of the upper and lower layers, respectively, would be 1.0 if the mixed fluid was homogeneous, but the mixing was inefficient in this sense as $(2\overline{\Delta\rho}/(\rho_2-\rho_1)) \approx 0.14 \pm 0.03$ for all experiments. More importantly, this definition enabled an appropriate Rossby deformation radius for the mixed fluid to be defined by $L_\mathrm{D} = [(g\overline{\Delta\rho}/\rho_1)h]^{\frac{1}{2}}/f$ where $f = 2\Omega$.

The mixed region initially spread axisymmetrically and from videotape records of 13 runs, the initial mean flow had a Rossby number of typically about 0.2 when non-axisymmetrical disturbances began to appear in time $t = (8.7 \pm 2.2)$ rotation periods after the commencement of stirring. At the onset of instability the azimuthal wavenumber ranged between 2 and 5 for the different runs. The ratio of the width of the current W at instability to the Rossby radius (W/L_D) was estimated as ranging between 2 and 5 and the initial depth ratio $(h/H) \approx 0.15$ (where H was the total depth).

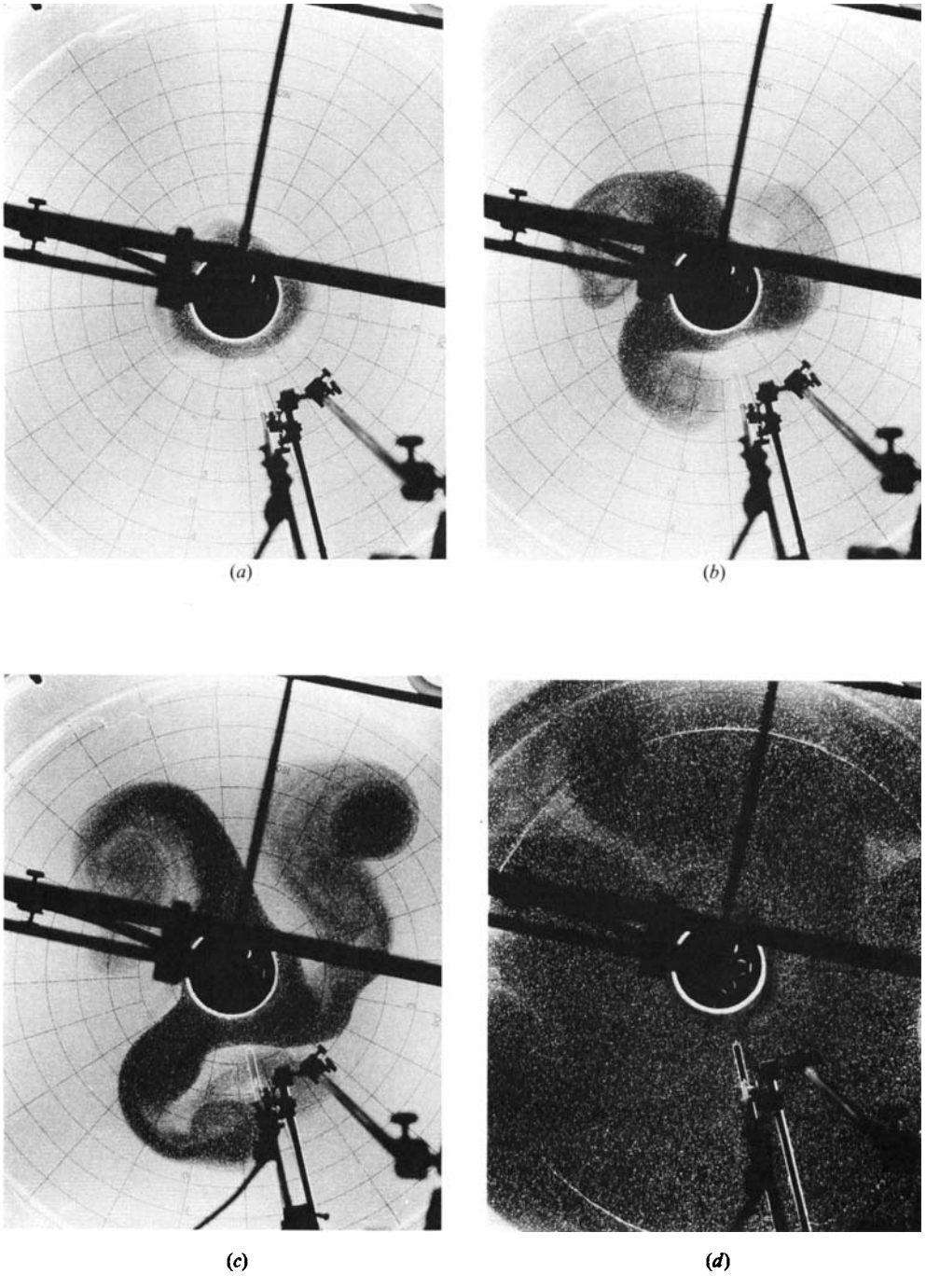

FIGURE 1. Photographic sequence from run 9 ($\Omega = 1.5$ rs^{-1} in the anticlockwise direction). The photographs were taken at (*a*) 13 (*b*) 26 (*c*) 39 (*d*) 179 rotation periods after the commencement of stirring. The bottom of the tank is marked with concentric circles 5 cm apart, and the radial lines are 15° apart.

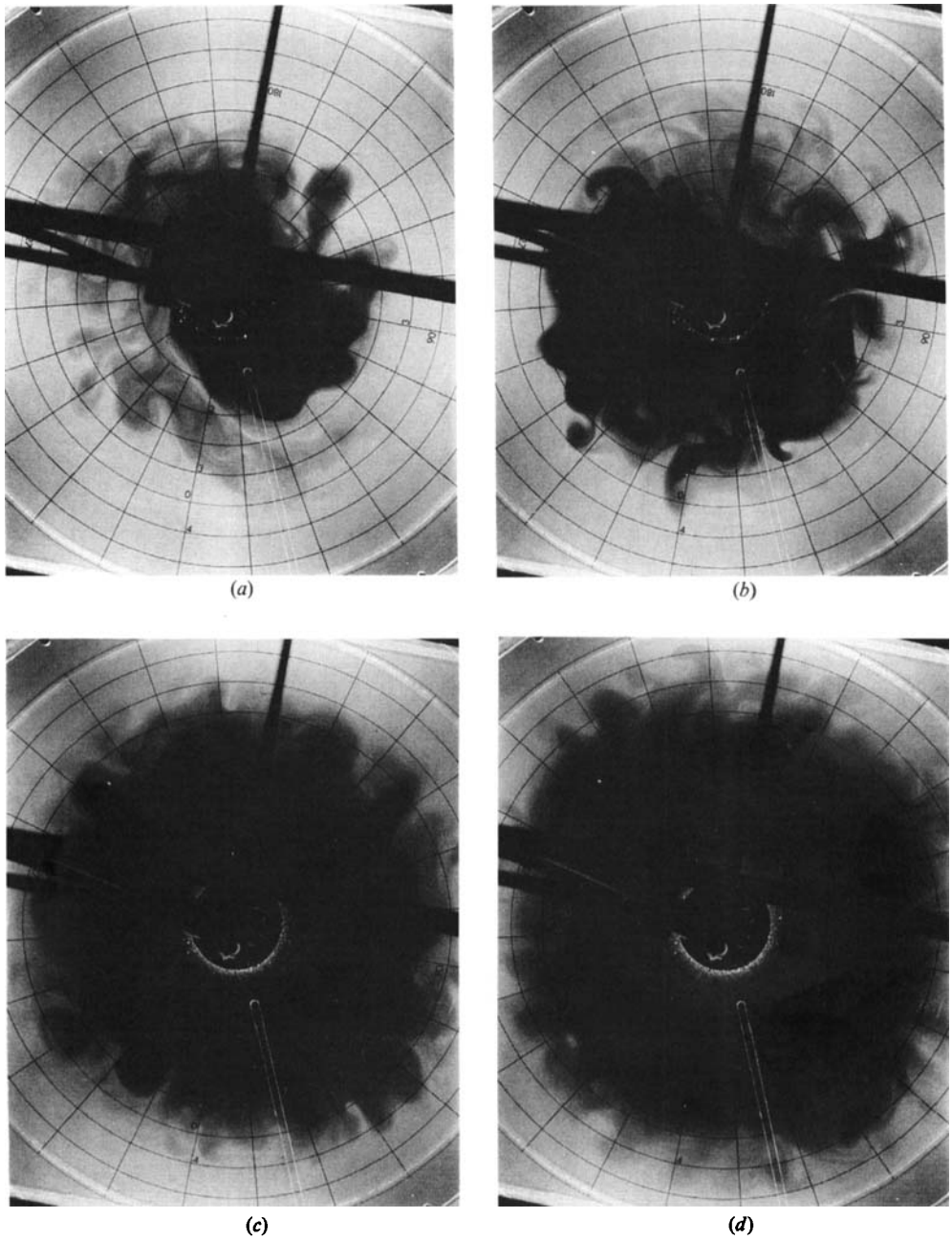

FIGURE 2. Photographic sequence from run 4 ($\Omega = 3$ rs^{-1} in the anticlockwise direction). The photographs were taken at (*a*) 79 (*b*) 104 (*c*) 230 (*d*) 286 rotation periods after the commencement of stirring.

Griffiths & Linden (1982) conducted an experiment designed to examine this class of rotational instabilities and suggested the existence of two regimes. If $W/L_{\mathrm{d}} > 3$, then the initial instabilities were baroclinic and the best estimate of their wavelength was $\lambda = 6.9L_{\mathrm{D}}$. Conversely, if $W/L_{\mathrm{D}} < 3$, then the initial instabilities were barotropic and the wavelength was $\lambda = 2.2W$. Since W/L_{D} ranged between 2 and 5 in the present

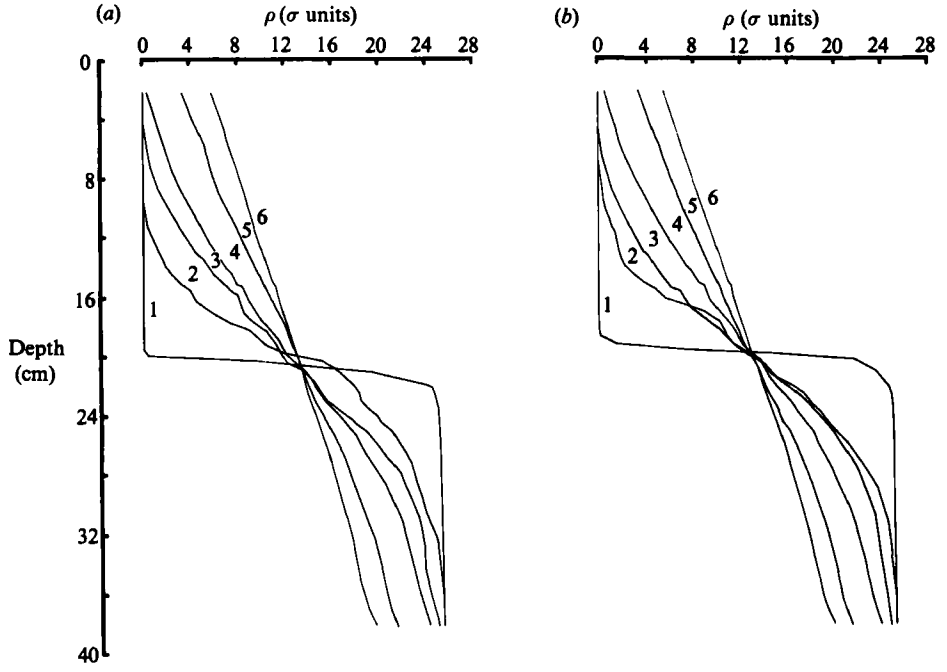

FIGURE 3. Evolution of the mean density gradient at two radial locations for run 6 ($\Omega = 1.0$ rs^{-1}). The positions were at (*a*) 10.2 cm and (*b*) 31.6 cm from the edge of the grid.

Profile	1	2	3	4	5	6
Time (min)	0.0	19.5	46.5	75.5	125.5	191.0

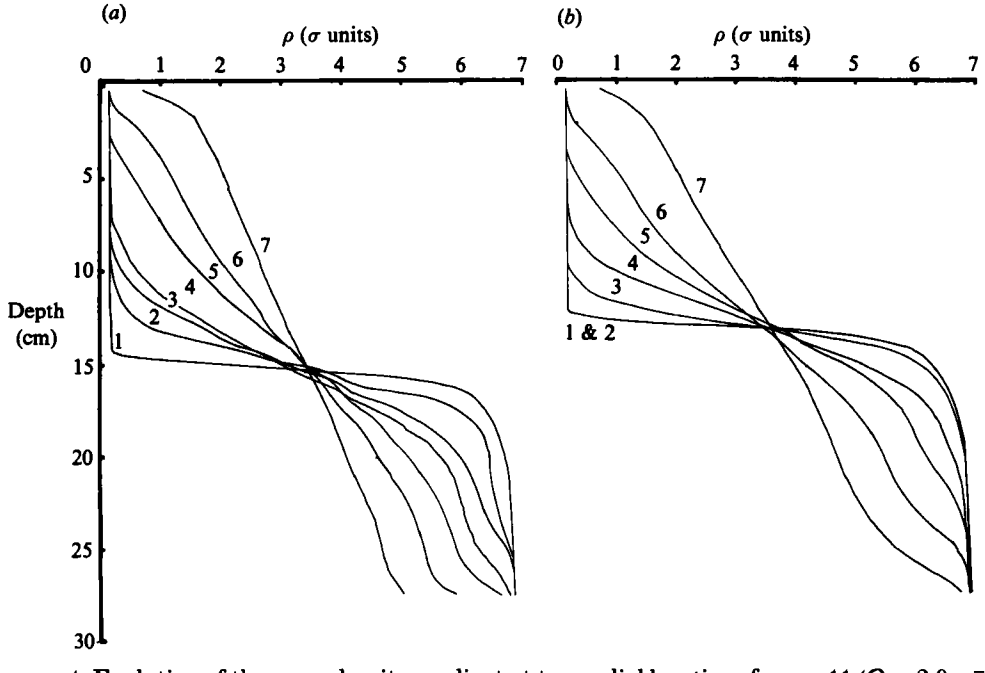

FIGURE 4. Evolution of the mean density gradient at two radial locations for run 11 ($\Omega = 2.0$ rs^{-1}). The positions were at (*a*) 10.2 cm and (*b*) 31.6 cm from the edge of the grid.

Profile	1	2	3	4	5	6	7
Time (min)	0.0	5.5	18.0	38.0	63.5	109.0	231.5

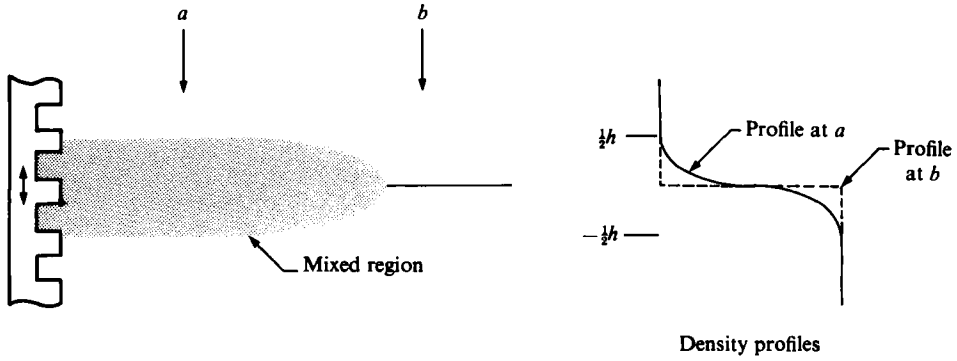

FIGURE 5. Vertical cross-sectional schematic of the initial collapse of the dyed mixed region.

experiments, it suggested the instabilities observed here were in a transitional range between the baroclinic and barotropic regimes.

The wavelength λ of the rotational instabilities was computed by dividing the circumference of the outer edge of the mixed region at the onset of instability by the observed azimuthal wavenumber (i.e. the number of disturbance crests). The experimental results indicated that this wavelength λ was given equally by $\lambda = (17 \pm 5) L_D$ or by $\lambda = (5 \pm 1) W$ and are clearly longer than those reported by Griffiths & Linden (1982). The two experiments were rather different in character: the earlier experiment, designed to examine rotational instabilities, employed the surface release of a fixed volume of buoyant fluid into an homogeneous environment, whereas the present experiment, designed to examine boundary mixing, produced a continuous internal intrusion of a partially mixed fluid between two homogeneous layers. Furthermore, this internal intrusion was driven by small-scale three-dimensional turbulent mixing (see §3.3 below), and this suggests a possible explanation of the present observations.

In such an active mixing situation, potential vorticity was not conserved, and by comparison with a situation with little or no mixing, the relative vorticity gained by the spreading fluid was smaller. The current was thus shallower and wider before it went unstable and for a given azimuthal mode number the wavelengths of the rotational instabilities were thus longer. The important point for the present experiments, however, was that due to an initial mixed mode instability, the spreading mixed region goes unstable in all cases.

At longer times the photographic sequence in figures 1 and 2 demonstrated that the instabilities grew and eventually broke down to produce a region of chaotic eddy motions filling the spreading mixed fluid. Little quantitative information is available about the rate of horizontal mixing due to mesoscale eddy motions and it is thus of interest to compare the present results with those from the experiments of Griffiths & Hopfinger (1984). They released a fixed volume of dyed buoyant fluid at the surface of a homogeneous dense environment and observed the subsequent spreading of the buoyant fluid. An initial baroclinic instability led to chaotic eddy motions filling the buoyant fluid and this dyed fluid was observed to eventually grow linearly in size with time. During this phase the turbulence could be described by a diffusion process with a constant horizontal diffusion coefficient whose magnitude was estimated from three runs all with $f = 2$ rs^{-1} as $K_H = 0.59\,(g'h/f)$. (Note that Griffiths & Hopfinger's equation (10) and hence their equation (A 2) is missing a factor of

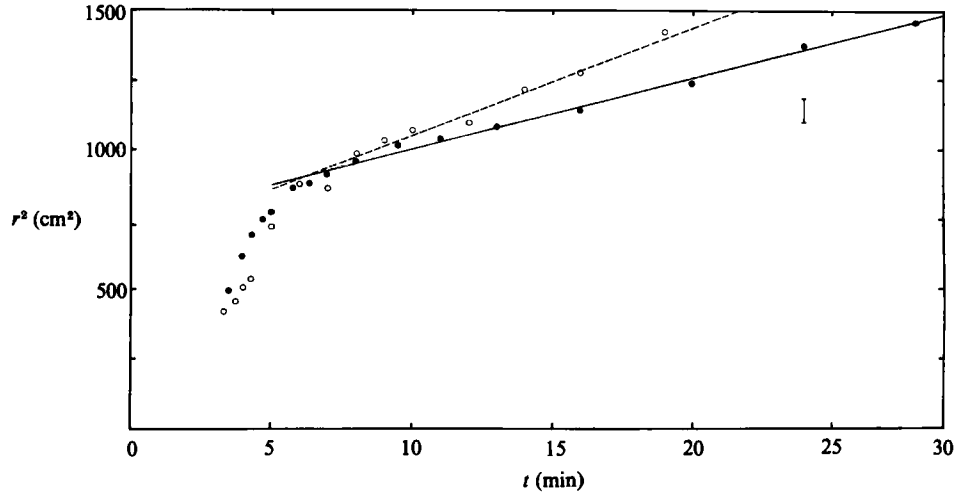

FIGURE 6. Size of the horizontally diffusing dye cloud as a function of time after the commencement of stirring. ●, run 12 ($\Omega = 3$ rs^{-1}); ○, run 13 ($\Omega = 2.5$ rs^{-1}). The size of the cloud is measured from the centre of the tank and the error bar is the estimated accuracy of individual estimates shown.

$(1/2\pi)$ where g' and h refer to the initial gravitational anomaly and depth of the spreading, buoyant volume of fluid.)

It was possible to make a similar measurement in the present experiments from the observed spreading of the dyed, grid-mixed fluid propagating out along the original density interface. Figure 6 shows the results for the size of the diffusing cloud as a function of time for the two experiments with the highest rotation rates. In both cases after the radius of the cloud exceeded approximately 30 cm (i.e. 25 cm from the grid), the experiments exhibited a near-linear growth of cloud size with time. The strength of both the grid stirring and the initial stratification was the same in the two runs, and the figure demonstrates that increasing the rotation rate reduces the rate of spreading of the cloud.

While no attempt was made to measure any turbulent velocity or lengthscales of the eddy field, we can follow Griffiths & Hopfinger (1984) and compute a horizontal turbulent diffusion coefficient from the data for the linear growth phase of the spreading cloud. (In the other runs at lower rotation rates the growing cloud did not attain a clearly defined linear growth phase before the finite size of the tank was encountered.) For comparison with Griffiths & Hopfinger (1984), we use initial values of $g' = g\overline{\Delta\rho}/\rho_1$ and h, where $\overline{\Delta\rho}$ and h are defined above and in figure 5, and the results in figure 6 then yield $K_H = C(g'h/f)$ where $C = 0.12$ and 0.14 for the two runs. The results of the two laboratory studies are thus in reasonable agreement, and while the two data sets are rather limited, suggest an average value of the turbulent diffusivity $K_H \approx 0.4\,(g'h/f)$ is representative for describing the horizontal or lateral mixing due to the mesoscale eddies.

3.3. *Vertical mixing*

The earlier boundary-mixing experiments of IC demonstrated the grid-generated turbulence was confined to a region of horizontal extent l_F adjacent to the grid. While the grid used in the experiments of IC was of unique design, Thorpe (1982) suggested it might have similar turbulence characteristics to the type employed by Hopfinger & Toly (1976). His suggestion proves compelling, and in the light of our own flux

measurements (see below), we propose only a slight modification in the dependence on the amplitude of grid oscillation. Let us assume that the induced turbulent velocity u and the integral lengthscale l are given by

$$u = \frac{C_A \omega a^{1.8} M^{0.2}}{r^*}, \quad l = \beta_A r^*, \tag{1}$$

where ω is the frequency of grid oscillation, a the amplitude of grid oscillation, M is the mesh size (2.54 cm) and $r^* = r - r_g$ is the radial distance from the grid (of radius $r_g = 5.5$ cm). With this assumption, the axisymmetric grid used in the present experiments has characteristics which indicated best estimates of the constants in (1) were $C_A = 0.16$ and $\beta_A = 0.19$ (see Appendix).

Since the strength of the turbulence decreases with distance from the grid, there will be a point at which buoyancy suppresses the overturning motion. This is the location of the turbulent front and its width l_F is given by the distance from the grid where

$$l_F = 1.7 L_B, \tag{2}$$

where the Ozmidov scale $L_B = (\epsilon/N^3)^{\frac{1}{2}}$ and the dissipation $\epsilon = u^3/l$. The constant 1.7 arises from the observations of Itsweire, Helland & Van Atta (1986). Substituting (1) into (2) we find the frontal position

$$r = l_F = (1.7)^{0.33} \left(\frac{C_A}{\beta_A}\right)^{0.5} M^{0.1} a^{0.9} \left(\frac{\omega}{N}\right)^{0.5}. \tag{3}$$

In the earlier experiments, IC argued that the vertical turbulent density flux per unit width F_2 was confined within this turbulent front of width l_F and as a consequence

$$F_2 = \left[\int_0^L \overline{w'\rho'}\,\mathrm{d}x\right]_{z_0} = \left[\int_0^{l_F} \overline{w'\rho'}\,\mathrm{d}x\right]_{z_0} = \left[\frac{\mathrm{d}}{\mathrm{d}t}\int_{z_0}^H \rho\,\mathrm{d}z\right] L, \tag{4}$$

where L is the tank length, x is distance from the grid and z_0 a reference elevation.

Within the turbulent region, the fluid behaves like a region of neutral stability (e.g. Stillinger, Helland & Van Atta 1983; Itsweire *et al.* 1986), and we can, therefore, define an effective eddy diffusivity within this region of the form

$$K = \alpha u l, \tag{5}$$

where α is a constant. Thus from (4) and (5)

$$F_2 = K\left(\frac{\rho_0}{g} N^2\right) l_F,$$

or using (1), (3) and (5) we obtain the prediction that

$$F_2 = B\left(\frac{\rho_0}{g}\right) \omega^{1.5} M^{0.3} a^{2.7} N^{1.5}, \tag{6}$$

where the constant $B = \alpha C^{1.5} \beta^{0.5} (1.7)^{0.33}$. This derivation is slightly different, but the result in (6) is entirely analogous to Thorpe's (1982) prediction in his equation (28). IC found a best fit to their data of the form

$$F_2 \propto \omega^{1.6} a^{2.7} N^{1.52}, \tag{7}$$

which is in close accord with the prediction in (6).

The additional external parameter in the present experiments is the rotation rate Ω, and the range of experimental values are tabulated in table 1. Conductivity

measurements and hence estimates of the vertical density flux were made for runs 6 to 14. In the axisymmetric configuration in these experiments, (4) takes the form

$$F = \left[2\int_{r_g}^{r_g+l_F} \overline{w'\rho'}\, r\, \mathrm{d}r \right]_{z_0} = \left[\frac{\mathrm{d}}{\mathrm{d}t} \int_{z_0}^{H} \rho\, \mathrm{d}z \right] (L^2 - r_g^2), \tag{8}$$

where L is the tank radius (50 cm) and we have assumed that, as in the non-rotating case, the vertical density flux is confined to the turbulent front (see below). Since the present experiments used the same type of grid as that employed by IC, we would expect by analogy with (6) above that (8) becomes

$$F = \left[B_A \left(\frac{\rho_0}{g} \right) \omega^{1.5} M^{0.3} a^{2.7} N^{1.5} \right] (2r_g + l_F) = \left[\frac{\mathrm{d}}{\mathrm{d}t} \int_{z_0}^{H} \rho\, \mathrm{d}z \right] (L^2 - r_g^2). \tag{9}$$

Using the values of C_A and β_A determined for the axisymmetric grid, the constant $B_A = 0.033\alpha$.

In the present experiments with rotation the vertical density flux F may thus be estimated by evaluating the right-hand side of (9). As in IC, this was done by a finite-difference approximation between successive conductivity profiles. The lower limit of integration z_0 for each conductivity probe (located at different radii) was taken as the elevation where successive conductivity profiles intersected (see figure 3, for example). This accounted for both the never perfect two-layer stratification and for the slope of the isopycnals at high rotation rates.

The buoyancy frequency N is one of the most important independent variables and the dependence of F on N^2 is shown in figures 7 (*a*) and 7 (*b*) where the rotation rate $\Omega = 1$ rs^{-1} for all the data. As in IC, N was evaluated from the local slope of the density versus depth trace at the elevation $z = z_0$. The rather limited data set in figure 7 (*a*) has a best fit straight line of slope $n = 0.71 \pm 0.17$, while the much more extensive data set in figure 7 (*b*) has a slope $n = 0.80 \pm 0.06$ (the error bounds represent the 90 % confidence limits). The mean estimates of the slopes are thus consistent with the prediction of $F \propto N^{1.5}$ in (9). The rather limited data set in figure 7 (*a*) is presented to demonstrate the strong influence of varying the amplitude of oscillation a. Accepting that $F \propto N^{1.5}$, the data in figure 7 (*a*) with $a = 0.52$ cm yield a mean value of $F/N^{1.5} = 5.4 \times 10^{-5}$ kg s$^{0.5}$, while the data in figure 7 (*b*) with $a = 0.75$ cm yield a mean value of $F/N^{1.5} = 1.6 \times 10^{-4}$ kg s$^{0.5}$. This is only a limited range, but from these two estimates the data implies $F \propto a^n$ where $n = 2.8$, again in close accordance with the prediction in (9). No attempt was made to vary the frequency of oscillation. These results suggest, however, that for a given rotation rate the dependence of the vertical density flux F on grid forcing and stratification was entirely consistent with the earlier non-rotating experiments of IC using a similar grid.

The rotation rate was actually varied between 0 and 3 r/s for the various experimental runs tabulated in table 1. For the run with $\Omega = 0$ r/s, the behaviour was identical to that described in the previous experiments of IC, with a weakening of the vertical density gradient by slow basin-scale circulation. A secondary feature of the flow was a series of irregular small-scale intrusions also noted by IC, but these were not detected in the other runs with rotation – presumably because their signature is smeared by the rotational instabilities and resulting mesoscale turbulence. As seen in §3.1, for the runs with high rotation rates, radial density gradients developed, and in these cases (runs 11, 12 and 13) a slightly modified version of (9) was used in order to compute the vertical density flux F. Instead of the tank radius, the radius of the dyed, radially-spreading mixed fluid was used in the right-hand side

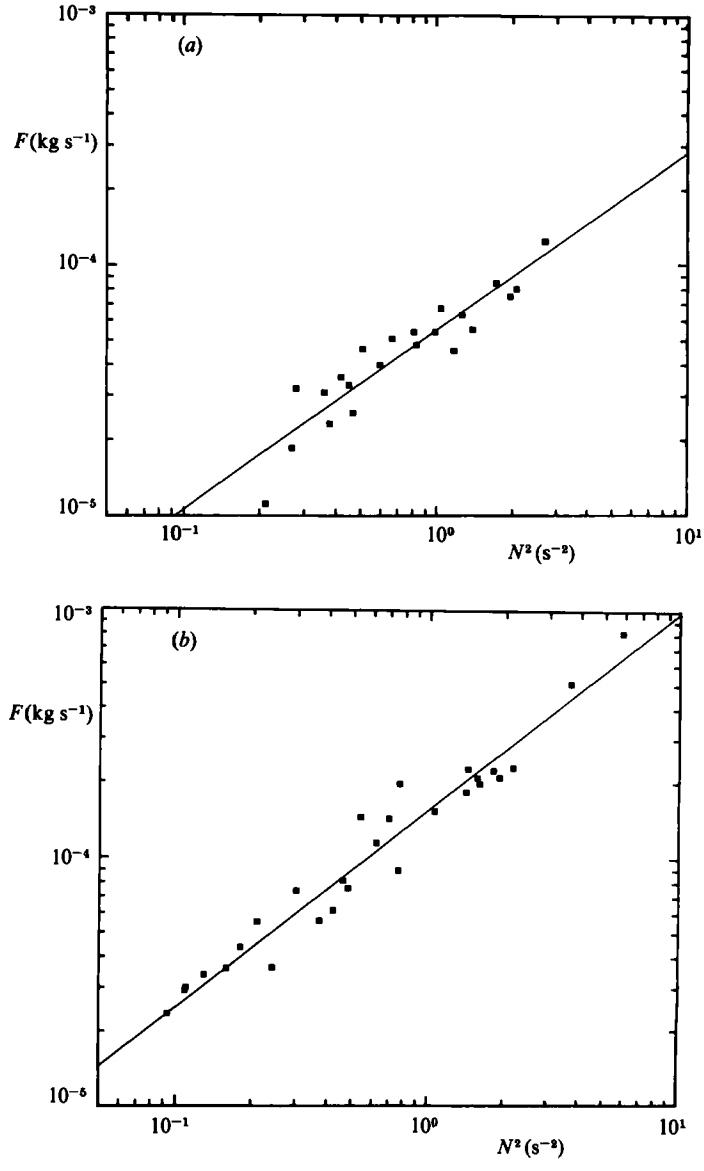

FIGURE 7. Vertical density flux F as a function of N^2 for grid amplitudes of oscillation of (*a*) 0.52 cm and (*b*) 0.75 cm with $\Omega = 1$ rs^{-1}.

of (9). This was determined from still photographs at the time of a given conductivity profile. A conductivity profile through the mixed region was then assumed representative of the entire dyed fluid. Once the mixed fluid had filled the tank, the average value from the two probes was used for the estimates of F. The results are shown in figure 8 which presents the measured vertical density fluxes for all runs.

The data points in figure 8 are all marked with their appropriate rotation rate. To the accuracy with which vertical fluxes could be determined, there appears to be no trend with increasing rotation rate and the results suggest that rotation has no influence on the rate of vertical mixing in the experiments.

This result implies the vertical turbulent density flux was restricted to the

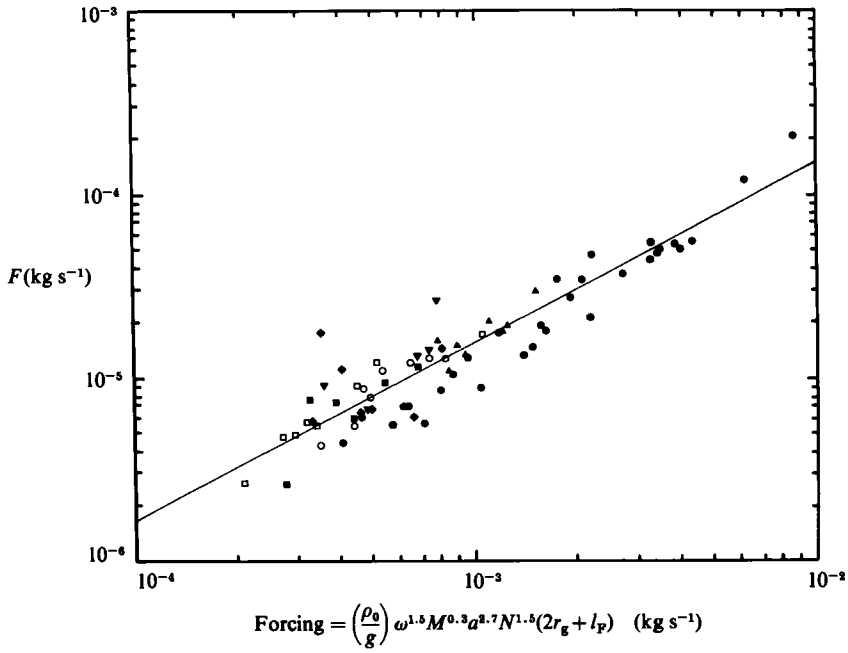

FIGURE 8. Summary of all experiments with observed vertical density flux F as a function of the forcing parameters in equation (9). The straight line indicates the linear correlation. Rotation rate (rs^{-1}): ○, 0.0; ■, 0.5; ●, 1.0; ▲, 1.5; □, 2.0; ▼, 2.5; ◆, 3.0.

turbulent region adjacent to the grid and the energetic small-scale turbulence driving the vertical mixing within this region was unaffected by the table rotation, as assumed in deriving (9) above. In terms of vorticity, the magnitude of the local turbulent vorticity fluctuations due to the grid oscillation were large compared to the relative vorticity the fluid may acquire due to mean motion in the rotating reference frame. The field of mesoscale eddies evidently accomplishes a negligible amount of vertical mixing compared to the vertical mixing within the turbulent region adjacent to the grid. The data plotted in figure 8 are seen to be in reasonable agreement with the prediction in (9) over an extensive parameter range. They suggest the constant in (9) is $B_A \approx 0.015$ which, in turn, suggests the constant in the expression for eddy diffusivity in (5) has a value of $\alpha = 0.42$ (a plausible value which thus provides an additional check on the consistency of the above formulation and its applicability in describing the experimental results). While rotation does not influence the rate of vertical mixing, it does play a dominant role in redistributing the mixed fluid generated by the continual grid stirring throughout the tank due to the horizontal mixing by the mesoscale eddies, and hence, on the temporal and spatial evolution of the interior density gradient.

4. Discussion of results

Since rotation plays no role in determining the vertical mixing rate in the laboratory experiments, the overall parameterization of that vertical mixing is the same for the present experiments as for the earlier non-rotating experiments of IC. IC introduced a vertical adjustment time scale T_2 representing the time it takes for

the interior density gradient to change in response to a mixing process at the boundary. For the case of a linear stratification N, this timescale was defined as

$$T_2 \sim \left[\frac{1}{N^2}\frac{\mathrm{d}}{\mathrm{d}t}(N^2)\right]^{-1},$$

and with the functional dependence in (6) and (9) above, this takes the form (cf. IC equation (30))

$$T_2 \sim \frac{N^{0.5}H^{2.0}L}{\omega^{1.5}M^{0.3}a^{2.7}} \sim \left(\frac{H^{2.0}}{\omega M^{0.2}a^{1.8}}\right)\left(\frac{L}{M^{0.1}a^{0.9}\omega^{0.5}N^{-0.5}}\right).$$

We see now from (1) and (5) that the eddy diffusivity in the turbulent region K has the form

$$K \sim \omega M^{0.2}a^{1.8}, \tag{10}$$

and using (3), the timescale T_2 is simply

$$T_2 \sim \left(\frac{H^2}{K}\right)\left(\frac{L}{l_F}\right). \tag{11}$$

The vertical adjustment timescale T_2 is thus equivalent to the vertical diffusion timescale in the turbulent region multiplied by the ratio of tank width to the turbulent frontal width. If the turbulence were energetic enough to fill the tank $L/l_F \sim 1$ and, as expected, one finds the vertical adjustment timescale is simply the depth of the fluid divided by the average vertical diffusion coefficient representative of the whole tank, the one-dimensional vertical diffusion timescale.

There is also a characteristic horizontal adjustment timescale which, in the absence of rotation, is given by (IC §6)

$$T_1 \sim L/u_0, \tag{12}$$

where u_0 is the characteristic velocity of fluid pumped out of the turbulent region. In the presence of rotation, on the other hand, the results of §3.1 indicate the horizontal adjustment can be described by a rotationally-dependent horizontal eddy diffusivity K_H. We can thus define a horizontal adjustment timescale T_1 in this case by

$$T_1 \sim L^2/K_H. \tag{13}$$

A comparison of the vertical adjustment timescale T_2 and the horizontal adjustment timescale T_1 then affords a simple interpretation of the range of behaviours discussed in §3.1. If timescale T_2 is long compared to timescale T_1, then horizontal mixing processes will rapidly distribute boundary-mixed fluid over the tank, and no appreciable horizontal density gradients will be found. The vertical density gradient should be weakened uniformly throughout the tank (as seen in figure 3, for example). Conversely, if timescale T_2 is short compared to timescale T_1 (as happens, for example, for high rotation rates), horizontal density gradients will exist in the tank. While the vertical density gradient will still be eroded, as seen in figure 4, this will not occur at a uniform rate throughout the tank.

While the erosion of the vertical density gradient thus involves a two-dimensional process which is only truly turbulent diffusive within the turbulent front, it is possible to describe the overall mixing by an apparent basin-scale vertical diffusion coefficient K_{BASIN}. As IC noted, we can for example write $F_2 = K_{BASIN}(\rho_0/g)\,N^2L$ and thus from (6), we find

$$K_{BASIN} = B\frac{\omega^{1.5}M^{0.3}a^{2.7}}{N^{0.5}L}.$$

In view of (3) and (10), this can be written as

$$K_{\mathrm{BASIN}} = K\left(\frac{l_{\mathrm{F}}}{L}\right), \tag{14a}$$

or for the general configuration

$$K_{\mathrm{BASIN}} = K\left(\frac{A}{A_{\mathrm{BASIN}}}\right), \tag{14b}$$

where A is the horizontal area of the turbulent boundary region and A_{BASIN} the area of the entire basin. The above arguments demonstrate that if $T_2 > T_1$ then, in response to a boundary-mixing process, the interior density gradient adjusts uniformly throughout the tank or basin, and hence, the value of the apparent vertical diffusivity computed from (14) is appropriate for the whole basin.

No mention has yet been made of the effect of a sloping boundary and this aspect of the problem has recently been examined in the laboratory by Phillips, Shyu & Salmun (1986). They argued that within the turbulent boundary layer which forms along the slope there is a balance between along-slope advection and dispersion of the mean density gradient. This, in turn, produced a mean convergence in the boundary layer, and hence, an injection of boundary-mixed fluid into the interior. The overall behaviour of the system was quite similar to that observed in the earlier experiments of IC. The present study reveals that the addition of rotational effects does not influence the rate of vertical mixing. Thus, while the experiments of Phillips *et al.* (1986) were done in a non-rotating frame, their results can be incorporated directly into the above formulation.

The authors expressed their results as

$$F = 0.6\left(\frac{\rho_0}{g}\right) K^{\frac{3}{4}} N^{\frac{5}{4}} \frac{\cos^2\theta}{\sin^{\frac{3}{4}}\theta}.$$

They also argued, by analogy with the laminar case considered by Phillips (1970), that the turbulent boundary-layer thickness measured perpendicular to the boundary was $l_{\mathrm{F}} = (2K/N\sin\theta)^{\frac{1}{2}}$, and defining an effective basin scale diffusivity as above of $K_{\mathrm{BASIN}} = (g/\rho_0)\,F/(N^2 L)$, their results can thus be written in the form

$$K_{\mathrm{BASIN}} = K\left(\frac{l_{\mathrm{F}}}{L}\right)\frac{\cos^2\theta}{\sin\theta}, \tag{15a}$$

and in the limit of small slope θ this becomes

$$K_{\mathrm{BASIN}} = \frac{K}{\theta}\left(\frac{l_{\mathrm{F}}}{L}\right), \tag{15b}$$

where the order one constant has been absorbed into the definition of K without loss of generality. The reduced expression in (15*b*) is thus a simple geometrical generalization of the formulation in (14) above. The result in (15*b*) in fact proves to be the same as a relationship first proposed by Armi (1978) to describe boundary mixing in the deep ocean and for the case of small bottom slopes, the experiments thus appear to support his original hypothesis.

Can these results then be used for predicting the strength of boundary mixing in the field? In the laboratory, the oscillating mechanical grid provides a convenient means of reaching sufficiently high Reynolds numbers to create local turbulent mixing in the stratified flow which we have argued can be parameterized in terms of K and l_{F}. In the field, the turbulent boundary layer results from the interaction

of the interior flow (mean currents, internal waves or both currents and waves) with the boundary. There have been some suggestions for the dependence of boundary-layer thickness l_F on flow properties and stratification (e.g. Weatherley & Martin 1978), but to date there appears to be no general theory available to parameterize K and l_F in terms of external parameters. This is particularly true in the case of breaking internal waves, which, in light of the energy arguments of Garrett (1979) and Eriksen (1985), seems the most likely mechanism for driving boundary mixing in the ocean.

While a better understanding of boundary-layer properties and their parameterization must await further field studies, it is nevertheless instructive to use typical numerical values of K and l_F from field studies. This assumes, as in the laboratory situation, that a near-boundary mixing event will create a local increase in potential energy relative to the interior, irrespective of the details of the driving mechanism. For the deep ocean for example, if we take $K = 10^{-2}$ m^2 s^{-1}, $l_F = 50$ m, $\theta = 0.005$ and $L = 3 \times 10^{-6}$ m, then (15b) implies $K_{BASIN} = 3 \times 10^{-5}$ m^2 s^{-1}. As Ivey (1986) argues, these parameter values are conservative, and thus the estimate of K_{BASIN} is likely to be an upper bound. Note that with the additional estimate of $H = 3 \times 10^3$ m for the deep ocean and assuming the horizontal distribution of boundary-mixed fluid is entirely by mesoscale diffusive processes with a $K_H = 10^3$ m^2 s^{-1} (mean currents may also assist in this distribution process), the horizontal mixing timescale $T_1 \sim L^2/K_H = 9 \times 10^9$ s, which is short compared to the vertical mixing timescale $T_2 = H^2/K_{BASIN} = 1.4 \times 10^{11}$ s, and the estimate of K_{BASIN} should thus be representative of the entire basin.

The above estimate of K_{BASIN} is plausible although somewhat smaller than Munk's (1966) estimate of $K_{BASIN} = 1 \times 10^{-4}$ m^2 s^{-1}. It must be emphasized that we cannot exclude the possibility that other mechanisms, such as internal wave breaking in the interior of the basin (e.g. Gargett 1984) may also contribute to K_{BASIN}, and the present estimate of K_{BASIN} is for the case of boundary-mixing operating alone. Furthermore, the result in (14) or (15) is simply a convenient way of expressing the overall vertical mixing by a two-dimensional adjustment process that leads to an apparent vertical diffusivity in the interior. While the estimates above are instructive, improved estimates of the role of boundary mixing are likely to come by focusing attention on the boundary-layer dynamics in the ocean, while measurements in the interior in the spirit of Moum & Osborn (1986) could well shed light on the relative importance of interior mixing compared to boundary mixing.

The present laboratory experiments and the observations of horizontal mixing may also be of relevance in understanding the dynamics of turbulent shelf fronts separating a well-mixed region from a two-layer stratification, such as observed in the Bering Sea (Schumacher *et al.* 1979) or around the British Isles (e.g. Simpson 1976). The field observations of mixing around islands in the Celtic Sea by Simpson *et al.* (1982) indicate an internal intrusive flow of mixed water away from the island and into the pycnocline. The scales are sufficiently large that rotation is important and the mechanism appears analogous to the initial behaviour of the laboratory experiments described in §3.1 involving a mixing and subsequent radial internal intrusion into the surrounding two-layer fluid. The data indicate the fluid is well mixed in the vicinity of the island, and taking the associated lateral density anomaly as $\Delta\rho = 0.75\sigma$ and the depth of the pycnocline as $h = 15$ m, then from §3.2 the predicted lateral diffusivity with which mixed fluid could be diffused away from the island in the pycnocline is $K_H = 0.4\,(g'h/f) \approx 400$ m s^{-2}. It is obvious from the field data that the net mean flow has a strong influence on the distribution of island-mixed

water, and it is thus difficult to compare this prediction with the observations. No measurements were reported of the vertical diffusivity K close to the island, and thus we cannot estimate any large-scale effective vertical diffusivities from (14) or (15), for example, for the area. It seems clear from the field data, however, that the boundary mixing is responsible for the enhanced biological productivity in the area.

5. Conclusions

In the present rotating-reference-frame experiments small-scale turbulence was confined by buoyancy forces to a region adjacent to the grid. As in IC, the divergence of the vertical density flux within this region created a lateral density gradient which led to an initially symmetrical internal radial collapse of mixed fluid. Some nine rotation periods after the commencement of stirring, the mixed region went unstable to non-axisymmetric rotational disturbances of transitional character between baroclinic and barotropic instability. Due to the strong mixing, the wavelength of the instabilities was longer than observed in previous experiments. The growing rotational instabilities eventually broke down and their subsequent mutual interaction created a field of mesoscale eddies which drove a horizontal mixing process (§3.2). This mixing could be described by a turbulent diffusion equation with a rotationally-dependent horizontal eddy diffusivity.

The combination of continual turbulent stirring, resulting in local vertical mixing at the boundary, and horizontal mixing by mesoscale eddies led to an erosion of the interior density gradient. The mechanism had the appearance of a local one-dimensional vertical diffusion process; in reality it was a very two-dimensional process. While the rotation did not affect the rate of vertical mixing, it did influence the temporal and spatial evolution of the interior density gradient through the agency of the horizontal eddy diffusivity.

Arguments were presented to describe the mixing characteristics in terms of experimental parameters and were shown to be in good agreement with the observations (§3.3). With the application to natural water bodies in mind, it was shown these results could be generalized to yield a relatively simple generalized formulation for the mixing rates (§4). For either small or large water bodies and irrespective of the exact nature of the forcing, the overall mixing could be described in terms of a turbulent eddy diffusivity at the boundary, a characteristic width of the turbulent boundary region, and the overall basin dimensions.

A preliminary version of this paper was presented at the IUTAM Symposium on Mixing in Stratified Fluids at Margaret River, Western Australia in August, 1985. The author would like to thank Derek Corrigan and Pat Travers for their efforts in the design and construction of the experimental facility, Scott Condie for his assistance in performing the experiments, Ross Wylde-Browne for help with the photography, and Karen Buckley for typing the paper.

Appendix

Two independent measurements were made in order to determine the two unknown constants C_A and β_A in equation (1) for the axisymmetric grid used in these experiments. Firstly, direct estimates were made of the turbulent velocities. This was accomplished by seeding a homogeneous fluid with small polystyrene particles. The flow was visualized by slit-lighting an approximately 1 cm wide vertical radial plane.

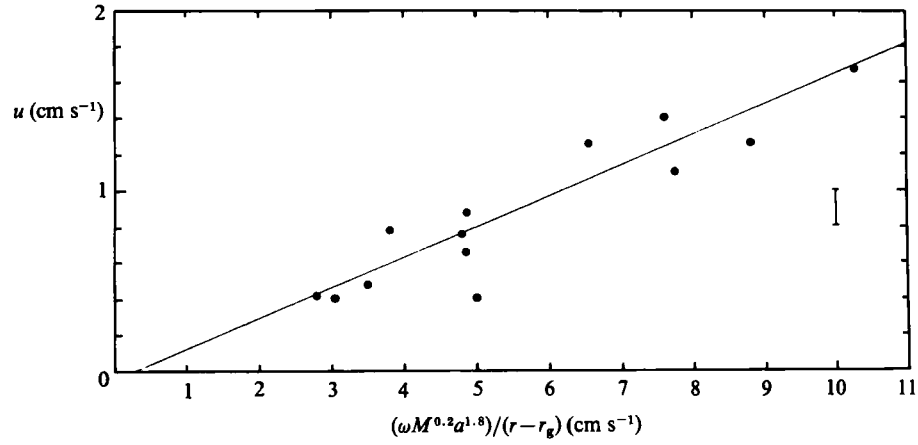

FIGURE 9. Turbulent velocities measured from streak photographs as a function of grid parameters in equation (1). All data for $r \geqslant 1.5M$ from the grid where the error bar is representative of one standard deviation either side of the individual estimates shown.

Streak photographs were then taken of the motion of the polystyrene particles for varying grid parameters and velocities inferred from the streak lengths and exposure times. Representative velocities were computed by taking the average over a number of streaks (usually about 25) in the same local area. The method proved too crude to evaluate the individual dependencies on ω and a, for example, over the limited parameter range available (see below). Consequently, the results shown in figure 9 summarize all the data where velocity u is plotted against $\omega a^{1.8}M^{0.2}/r$ from equation (1). The best fit straight line shown has a slope of 0.165, but a realistic estimate implies the constant $C_A = 0.16 \pm 0.03$ for the data shown.

A second quantity of fundamental interest in these experiments is the width of the turbulent frontal region l_F surrounding the grid and a series of experiments were conducted to measure l_F. The tank was filled with a linearly stratified fluid seeded with a uniform distribution of Kalliroscope AQ 1000 tracer during the filling process. The flow was again visualized by slit-lighting a 1 cm wide vertical radial plane. The mean width of the turbulent frontal region was then estimated from still and cine film of the tracer motion after starting the grid stirring. Figure 10 summarizes the results where the observed width l_F is plotted against $M^{0.1}a^{0.9}(\omega/N)^{0.5}$ from equation (3). Each data point represents a mean over approximately 20 observations. As Ivey (1980) first noted, turbulent eddies cause distortions about the mean frontal position – for a typical width of 7 cm from figure 10, the distortions are of order ± 1 cm about the mean position. The best fit straight line to the data shown in figure 10 has a slope 1.05 and from equation (3), with $C_A = 0.16$, the data in figure 10 imply $\beta_A = 0.19 \pm 0.04$.

These results do not provide an independent test of the assumption in (1) that the present grid behaves similarly to other grids of known properties as Thorpe (1982) first suggested. They do demonstrate, however, that the observations of grid properties are consistent with the assumption and yield plausible values of the coefficients C_A and β_A by comparison with more precise calibration of other grids (cf. Hopfinger & Toly 1976). As §3.3 demonstrates, they also lead to predictions in close agreement with the observed vertical mixing rates. One final point emerging from these tests is that the laws have a definite range of validity. There appears to be a

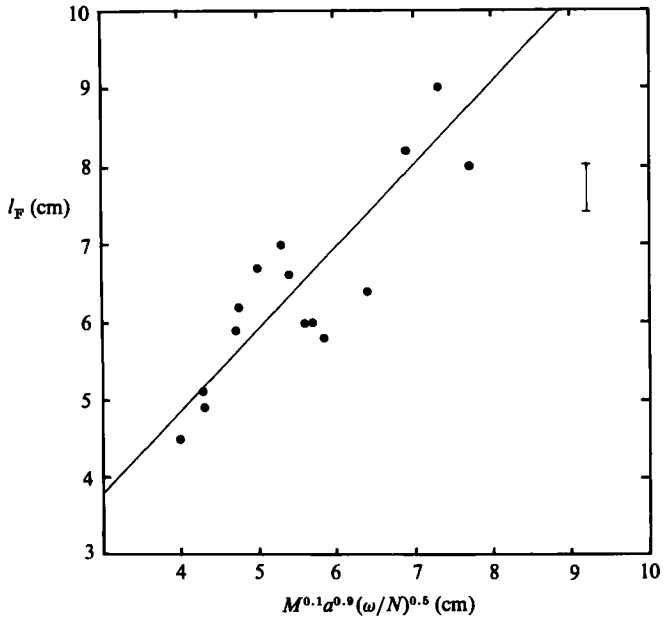

FIGURE 10. Mean width of the turbulent region l_F as a function of grid parameters and density stratification described in equation (3) where the error bar is representative of one standard deviation either side of the individual estimates shown.

lower limit beyond which there is an effect of the mesh size on the scale of the turbulence. Similarly, there is an upper limit beyond which the velocity law breaks down. These observations may be summarized by noting that over the range of grid Reynolds number $Re_g = (\omega a) M/\nu$ between approximately 5×10^3 to 10×10^3, the axisymmetric grid has properties consistent with those proposed in (1), with best estimates of $C_A = 0.16$ and $\beta_A = 0.19$ and an accuracy of about 20%.

REFERENCES

ARMI, L. 1978 Some evidence for boundary mixing in the deep ocean. *J. Geophys. Res.* **83**, 1971–1977.

ARMI, L. 1979 Effects of variation in eddy diffusivity on property distributions in the deep ocean. *J. Mar. Res.* **37**, 515–530.

CALDWELL, D. R., BRUBAKER, J. M. & NEAL, V. T. 1978 Thermal microstructure on a lake slope. *Limnol. Oceanogr.* **23**, 372–374.

DICKSON, R. R. & MCCAVE, I. N. 1986 Nepheloid layers on the continental slope west of Porcupine Bank. *Deep-Sea Res.* **33**, 791–818.

ERIKSEN, C. C. 1985 Implications of ocean bottom reflections for internal wave spectra and mixing. *J. Phys. Oceanogr.* **15**, 1145–1156.

GARGETT, A. E. 1984 Vertical eddy diffusivity in the ocean interior. *J. Mar. Res.* **42**, 359–393.

GARRETT, C. 1979 Comment on: Some evidence for boundary mixing in the deep ocean by L. Armi. *J. Geophys. Res.* **84**, 5095–5096.

GREGG, M. C. & SANFORD, T. M. 1980 Signatures of mixing from the Bermuda slope, the Sargasso Sea and the Gulf Stream. *J. Phys. Oceanogr.* **10**, 105–127.

GRIFFITHS, R. W. & LINDEN, P. F. 1982 Laboratory experiments on fronts. Part 1: Density-driven boundary currents. *Geophys. Astrophys. Fluid Dyn.* **19**, 159–187.

GRIFFITHS, R. W. & HOPFINGER, E. J. 1984 The structure of mesoscale turbulence and horizontal spreading at ocean fronts. *Deep Sea Res.* **31**, 245–269.

HOPFINGER, E. J. & TOLY, J. A. 1976 Spatially decaying turbulence and its relation to mixing across density interfaces. *J. Fluid Mech.* **78**, 155–175.

IMBERGER, J. 1985 Thermal characteristics of standing waters: an illustration of dynamic processes. *Hydrobiologia* **125**, 7–29.

ITSWEIRE, E. C., HELLAND, K. N. & VAN ATTA, C. W. 1986 The evolution of grid-generated turbulence in a stably stratified fluid. *J. Fluid Mech.* **162**, 297–338.

IVEY, G. N. 1980 Boundary mixing in density-stratified fluids. PhD thesis, University of California, Berkeley.

IVEY, G. N. 1986 The role of boundary mixing in the deep ocean. *J. Geophys. Res.* (submitted).

IVEY, G. N. & CORCOS, G. M. 1982 Boundary mixing in a stratified fluid. *J. Fluid Mech.* **121**, 1–26.

MCDOUGALL, T. J. 1986 Thermobaricity, cabbeling and the interpretation of microstructure dissipation data. *J. Geophys. Res.* (in press).

MARMORINO, G. O., DANOS, S. C. & MAKI, J. S. 1980 Temperature fine structure of Lake Michigan hypolimnion. *Limnol. Oceanogr.* **25**, 680–699.

MOUM, J. N. & OSBORN, T. R. 1986 Mixing in the main thermocline. *J. Phys. Oceanogr.* **16**, 1250–1259.

MUNK, W. 1966 Abyssal recipes. *Deep Sea Res.* **13**, 707–730.

PHILLIPS, O. M. 1970 On flows induced by diffusion in a stably, stratified fluid. *Deep Sea Res.* **17**, 435–443.

PHILLIPS, O. M., SHYU, J-H. & SALMUN, H. 1986 An experiment on boundary mixing: mean circulation and transport rates. *J. Fluid Mech.* **173**, 473–499.

SCHUMACHER, J. D., KINDER, T. H., PASHINSKI, D. J. & CHARNELL, R. L. 1979 A structural front over the continental shelf of the Eastern Bering Sea. *J. Phys. Oceanogr.* **9**, 79–87.

SIMPSON, J. H. 1976 A boundary front in the summer regime of the Celtic Sea. *Est. Coast. Mar. Sci.* **4**, 71–81.

SIMPSON, J. H., TETT, P. B., ARGOTE-ESPINOZA, M. L., EDWARDS, A., JONES, K. L. & SAVIDGE, G. 1982 Mixing and phytoplankton growth around an island in a stratified sea. *Cont. Shelf Res.* **1**, 15–32.

STILLINGER, D. C., HELLAND, K. N. & VAN ATTA, C. W. 1983 Experiments on the transition of homogeneous turbulence to internal waves in a stratified fluid. *J. Fluid Mech.* **131**, 91–122.

THORPE, S. A. 1982 On the layers produced by rapidly oscillating a vertical grid in a uniformly stratified fluid. *J. Fluid Mech.* **124**, 391–409.

WEATHERLY, G. L. & MARTIN, P. J. 1978 On the structure and dynamics of the oceanic bottom boundary layer. *J. Phys. Oceanogr.* **8**, 557–570.

WUNSCH, C. 1972 Temperature microstructure on the Bermuda Slope with application to the mean flow. *Tellus* **24**, 350–367.